The DØ Interacting Propagator

H. Greenlee

November 7, 2003

Contents

1 Introduction **2**

2 The Effect of Material on Charged Particle Motion **2**

2.1 Thin Multiple Scatterer . . . 2

2.1.1 Thin Cylindrical Multiple Scatterer . . . 3

2.1.2 Thin z-Plane Multiple Scatterer . . . 4

2.1.3 Thin xy-Plane Multiple Scatterer . . . 5

2.2 Thick Multiple Scatterer . . . 5

2.3 Energy Loss . . . 6

3 The Design and Implementation of `D0Propagator` **8**

3.1 PropCFT . . . 11

3.2 SMTPropagator . . . 11

3.2.1 SMT Barrels . . . 12

3.2.2 SMT F disks . . . 13

3.2.3 SMT Support Trough and Beampipe . . . 13

A TRF interactor classes **14**

A.1 Interactor . . . 14

A.2 MultiInteractor . . . 14

A.3 Thin multiple scattering interactors . . . 14

A.4 Thick multiple scattering interactors . . . 15

A.5 Energy loss interactors . . . 15

1 Introduction

This note describes the DØ interacting propagator `D0Propagator`. This class propagates tracks in the DØ detector, with error, including the effect of detector material. This note is a sequel to Ref. [1], which describes some of the theory and implementation of non-interacting propagators for DØ.

Section 2 of this note contains a general description of the effect of material on the propagation of charged particles in a magnetic field. This section is not strongly DØ-specific, although the situations considered are ones that are of interest to DØ. Section 3 deals specifically with the way in which the considerations of Sec. 2 are implemented in `D0Propagator`. Appendix A describes some of the trf classes that are used in support of `D0Propagator`.

2 The Effect of Material on Charged Particle Motion

In this section, we give the mathematical formulas that describe the effect of material on the motion of a charged particle. We consider the following three cases:

1. Thin multiple scatterer.
   The only effect is on the errors of the track angle parameters.

2. Thick multiple scatterer.
   The track position errors are also affected (in addition to the track angle errors).

3. Energy loss.
   The mean value of the track curvature (momentum) and the corresponding error are affected. The track position and angle are not affected regardless of the thickness of the material. For thick enough material, the change in the mean value of the momentum will eventually propagate to other track parameters via the magnetic curvature of the track, if any. Therefore, with a curving track, we must limit the thickness of the material for which we calculate energy loss.

The thin multiple scatterer is a special case of the thick multiple scatterer. We consider that multiple scattering and energy loss are independent effects. We also consider that the magnetic curvature of the track, if any, is irrelevant when calculating the effect of material.

2.1 Thin Multiple Scatterer

In real life, any physical multiple scatterer has a finite thickness. The thin multiple scattering approximation is valid if the material is thin enough so that multiple scattering does not contribute significantly to the error of the track position, as compared to other relevant position errors, such as the track position measurement errors. Multiple scattering in the region of the central tracking detectors is exclusively modeled in the thin scatterer approximation. The thin multiple scattering approximation is manifestly false for charged particles traversing extended material bodies, such as muons moving through iron or other dense material.

The basic formula for calculating the average deflection angle in a plane due to multiple scattering of a charged particle is as follows [2]:

$$\theta_0 = \frac{13.6\ \mathrm{MeV}}{\beta c p}\,|q|\,\sqrt{\frac{L}{L_R}}\left[1 + 0.038\log\left(\frac{L}{L_R}\right)\right], \tag{1}$$

where p is the momentum, βc is the velocity, $|q|$ is the charge number of the incident particle, and L is the thickness and L_R is the radiation length of the scatterer. The logarithm term represents the effect of additional tails being brought into the central peak of the Gaussian distribution of scattering angles as the thickness of the scatter is increased. Therefore, if a the total amount of multiple scattering material is divided among several smaller scatterers, it could be argued that the logarithm term should really be set using the total number of radiation lengths from all material, and the square root term should be the number of radiation lengths of the individual scatterers. However, the trf implementation uses Eq. 1 as is, using the same number of radiation lengths for both terms.

The angle θ_0 is the rms scattering angle projected onto a plane. In space, two orthogonal angle parameters each have an rms scattering angle of θ_0. If a particle is traveling in a direction characterized by angles θ and ϕ, using standard spherical coordinates, then the rms scattering angles in the θ and ϕ directions are as follows:

$$\sigma_\theta^2 = \theta_0^2, \tag{2}$$
$$\sigma_\phi^2 = \theta_0^2 \csc^2\theta. \tag{3}$$

In terms of the standard trf track angle parameters $\tan\lambda = \cot\theta$ and $\phi_D = \phi$, these equations become:

$$\sigma_{\phi_D}^2 = \theta_0^2 \sec^2\lambda, \tag{4}$$
$$\sigma_{\tan\lambda}^2 = \theta_0^2 \sec^4\lambda. \tag{5}$$

There is no correlation between scattering in the ϕ and θ or ϕ_D and $\tan\lambda$ directions.

2.1.1 Thin Cylindrical Multiple Scatterer

On a cylindrical shell, a track is described using standard trf cylindrical track parameters (ϕ, z, α, $\tan\lambda$, and $C_T = q/p_T$). The errors of the track angle parameters α and $\tan\lambda$ are increased by multiple scattering. The transverse curvature C_T is also affected through the connection of this parameter to $\tan\lambda$. Equations 4–5 are almost in a form that can be applied directly to trf cylindrical track parameters. It only remains to eliminate ϕ_D in favor of $\alpha = \phi_D - \phi$ and to calculate the effect on the transverse curvature $C_T = C\sec\lambda$ (where $C = q/p$ is the space curvature).

$$\sigma_\alpha^2 = \theta_0^2 \sec^2\lambda, \tag{6}$$
$$\sigma_{\tan\lambda}^2 = \theta_0^2 \sec^4\lambda, \tag{7}$$

$$\sigma^2_{C_T} = \left(\frac{\partial C_T}{\partial \tan\lambda}\right)^2 \sigma^2_{\tan\lambda}, \tag{8}$$

$$= \theta_0^2 C_T^2 \tan^2\lambda, \tag{9}$$

$$\sigma^2_{C_T \tan\lambda} = \left(\frac{\partial C_T}{\partial \tan\lambda}\right)\left(\frac{\partial \tan\lambda}{\partial \tan\lambda}\right) \sigma^2_{\tan\lambda}, \tag{10}$$

$$= \theta_0^2 C_T \tan\lambda \sec^2\lambda. \tag{11}$$

$$\tag{12}$$

Note that the correlation coefficient between C_T and $\tan\lambda$ is 1 or -1, depending on the sign of $C_T \tan\lambda$. The only other refinement that we need to take into account is to increase the scattering length L due to the incidence angle of the particle relative to the cylindrical scatterer:

$$L = L_0 \left|\sec\alpha\right| \sec\lambda, \tag{13}$$

where L_0 is the path length for normal incidence particles.

2.1.2 Thin z-Plane Multiple Scatterer

On a z-plane, a track is described using standard trf Cartesian track parameters (x, y, x', y', and $C = q/p$). The errors of the track angle parameters x' and y' are increased by multiple scattering. The Cartesian angle parameters are defined as follows in terms of ϕ_D and $\tan\lambda$:

$$x' = \cos\phi_D \cot\lambda, \tag{14}$$

$$y' = \sin\phi_D \cot\lambda. \tag{15}$$

The error matrix in the (x', y') basis is as follows:

$$\sigma^2_{x'} = \left(\frac{\partial x'}{\partial \phi_D}\right)^2 \sigma^2_{\phi_D} + \left(\frac{\partial x'}{\partial \tan\lambda}\right)^2 \sigma^2_{\tan\lambda}, \tag{16}$$

$$= \theta_0^2 \left(y'^2 \sec^2\lambda + x'^2 \sec^2\lambda \csc^2\lambda\right), \tag{17}$$

$$= \theta_0^2 \left(1 + x'^2\right)\left(1 + x'^2 + y'^2\right), \tag{18}$$

$$\sigma^2_{y'} = \theta_0^2 \left(1 + y'^2\right)\left(1 + x'^2 + y'^2\right), \tag{19}$$

$$\sigma^2_{x'y'} = \left(\frac{\partial x'}{\partial \phi_D}\right)\left(\frac{\partial y'}{\partial \phi_D}\right) \sigma^2_{\phi_D} + \left(\frac{\partial x'}{\partial \tan\lambda}\right)\left(\frac{\partial y'}{\partial \tan\lambda}\right) \sigma^2_{\tan\lambda}, \tag{20}$$

$$= \theta_0^2 \left(-x'y' \sec^2\lambda + x'y' \sec^2 \csc^2\lambda\right), \tag{21}$$

$$= \theta_0^2 x'y' \left(1 + x'^2 + y'^2\right). \tag{22}$$

The path length is

$$L = L_0 \sqrt{1 + x'^2 + y'^2}, \tag{23}$$

where L_0 is the path length for normal incidence particles.

2.1.3 Thin xy-Plane Multiple Scatterer

On an xy-plane, a track is described using standard trf rotated Cartesian track parameters (v, z, v', z', and $C = q/p$). The errors of the track angle parameters v' and z' are increased by multiple scattering. The Cartesian angle parameters are defined as follows in terms of ϕ_D and $\tan\lambda$:

$$v' = \tan(\phi_D - \phi_{xy}), \tag{24}$$
$$z' = \sec(\phi_D - \phi_{xy}) \tan\lambda, \tag{25}$$

where ϕ_{xy} is the azimuth of the normal direction to the xy plane. The error matrix in the (v', z') basis is as follows:

$$\begin{aligned}
\sigma^2_{v'} &= \left(\frac{\partial v'}{\partial \phi_D}\right)^2 \sigma^2_{\phi_D} + \left(\frac{\partial v'}{\partial \tan\lambda}\right)^2 \sigma^2_{\tan\lambda}, && (26)\\
&= \theta_0^2 \sec^4(\phi_D - \phi_{xy}) \sec^2\lambda, && (27)\\
&= \theta_0^2 \left(1 + v'^2\right)\left(1 + v'^2 + z'^2\right), && (28)\\
\sigma^2_{z'} &= \left(\frac{\partial z'}{\partial \phi_D}\right)^2 \sigma^2_{\phi_D} + \left(\frac{\partial z'}{\partial \tan\lambda}\right)^2 \sigma^2_{\tan\lambda}, && (29)\\
&= \theta_0^2 \Big[\sec^2(\phi_D - \phi_{xy}) \tan^2(\phi_D - \phi_{xy}) \sec^2\lambda \tan^2\lambda \\
&\quad + \sec^2(\phi_D - \phi_{xy}) \sec^4\lambda\Big], && (30)\\
&= \theta_0^2 \left(1 + z'^2\right)\left(1 + v'^2 + z'^2\right), && (31)\\
\sigma^2_{v'z'} &= \left(\frac{\partial v'}{\partial \phi_D}\right)\left(\frac{\partial z'}{\partial \phi_D}\right) \sigma^2_{\phi_D} + \left(\frac{\partial v'}{\partial \tan\lambda}\right)\left(\frac{\partial z'}{\partial \tan\lambda}\right) \sigma^2_{\tan\lambda}, && (32)\\
&= \theta_0^2 \sec^3(\phi_D - \phi_{xy}) \tan(\phi_D - \phi_{xy}) \tan\lambda \sec^2\lambda, && (33)\\
&= \theta_0^2 v' z' \left(1 + v'^2 + z'^2\right). && (34)
\end{aligned}$$

The path length is

$$L = L_0 \sqrt{1 + v'^2 + z'^2}, \tag{35}$$

where L_0 is the path length for normal incidence particles.

2.2 Thick Multiple Scatterer

The effect of multiple scattering on track angle parameters is independent of the physical thickness of the scatterer, being dependent only on the number of radiation lengths. If the material is thick enough however, the track position parameters are affected as well. According to Ref. [2], the position error induced by multiple scattering is $L/\sqrt{3}$ times the angle error for a scatterer of thickness L. The position error and angle error are uncorrelated if the scattering is assumed to take place at the center of the scatterer (i.e. halfway through).

2.3 Energy Loss

In a sense, the effect of energy loss is simpler than multiple scattering because it is only the track momentum that is affected, regardless of the thickness of the material. Of course, if the track is bending because of a magnetic field, fluctuations in momentum will eventually be propagated to angle and position. Since this effect is not included, in the formulas in this section, we should limit the thickness of material for which we calculate energy loss.

When calculating energy loss, we are concerned with the mean energy loss, and with energy loss fluctuations. The mean energy loss is described by the Bethe-Bloch equation [2, 3].

$$\frac{dE}{dx} = -\rho K z^2 \frac{Z}{A} \frac{1}{\beta^2} B(\beta), \tag{36}$$

where ρ is the density of the material, z is the charge number of the incident particle (henceforth assumed to be one), Z and A are the atomic number and atomic mass of the material, and K is a constant given by

$$K = 4\pi N_A r_e^2 m_e c^2 = 0.307075 \text{ MeV cm}^2 (/\text{mol}). \tag{37}$$

Note that while we consider Z to be a pure number, A has units of g/mol, giving the correct units of MeV/cm for dE/dx.

$B(\beta)$ is called the stopping number. It is given by the following formula:

$$B(\beta) = \frac{1}{2} \log \frac{2m_e c^2 \beta^2 \gamma^2 T_{\max}}{I^2} - \beta^2 - \frac{1}{2}\delta, \tag{38}$$

where I is the ionization energy of the atoms in the material, $T_{\max}$ is the maximum kinetic energy transfer to a free electron, and δ represents the "density effect" (see below). $T_{\max}$ is given by the following formula:

$$T_{\max} = \frac{2m_e c^2 \beta^2 \gamma^2}{1 + 2\gamma m_e/M + (m_e/M)^2}, \tag{39}$$

$$\simeq 2m_e c^2 \beta^2 \gamma^2, \tag{40}$$

where M is the mass of the incident particle. The approximate form of $T_{\max}$ (Eq. 40) is valid for $\gamma \ll M/m_e$. While it is certainly true that the approximate form is valid for most particles detected by the DØ trackers, it is not valid for the highest energy particles that are of interest to DØ. In the words of Ref. [2] "The correct expression should be used." It may be surprising that in the ultra-high-energy limit ($\gamma \gg M/m_e$) the maximum energy transfer is $T_{\max} \simeq \gamma M c^2$, or in other words, the incident particle can give up essentially all of its kinetic energy to an electron. For a 1 GeV pion, the maximum energy transfer is about 50 MeV. For a 50 GeV muon, the maximum energy transfer is about 40 GeV.

The density effect can be parameterized as follows [2]:

$$\delta = \begin{cases} 2(\log 10)x + C & \text{if } x \geq x_1; \\ 2(\log 10)x + C + a(x_1 - x)^k & \text{if } x_0 \leq x \leq x_1; \\ 0 & \text{if } x \leq x_0 \end{cases}, \tag{41}$$

where $x = \log_{10}(\beta\gamma)$ and the other parameters in Eq. 41 (C, a, k, x_0, and x_1, along with ρ, Z, A, and I) are dependent on the material.

The main features of Eq. 36 are well known. For relativistic particles (above the $1/\beta^2$ falloff), the dependence of the mean energy loss on the incident particle energy and type is weak, rising logarithmically with energy (relativistic rise). Apart from the linear dependence of energy loss on the material density (or more precisely, on the number density of electrons $N_A\rho Z/A$), the dependence on other material parameters is also weak.

Any attempt to quantify energy loss fluctuations in terms of a Gaussian standard deviation is necessarily very approximate, due to the large "Landau tail" of the energy loss distribution. Nevertheless, we are forced to adopt such an approximation because of the "error matrix" formalism that is used to describe tracks. One such approximation, which can be found in Ref. [3] for the variance of the energy loss for path length Δx is the following:

$$\sigma_E^2 = \gamma^2\left(1 - \frac{1}{2}\beta^2\right) m_e c^2 \frac{Z}{A} K\rho\,|\Delta x|\,. \tag{42}$$

Having calculated the mean energy loss $\Delta E = (dE/dx)/\Delta x$ (Eq. 36) and the standard deviation of the energy loss σ_E (Eq. 42) for a particular layer of material, we can now proceed to calculate the effect on the track parameters and error matrix. Only the curvature (or transverse curvature) is affected. The momentum of the particle is decreased (increased) for a particle being propagated in the forward (backward) direction. The error is always increased regardless of the direction of propagation. The contribution to the error of the curvature is as follows:

$$\sigma_C^2 = \left(\frac{\partial C}{\partial E}\right)^2 \sigma_E^2, \tag{43}$$

where the curvature parameter C is given by

$$\begin{aligned} C &= \frac{q}{p}, && (44)\\ &= \frac{q}{\sqrt{E^2 - M^2}}. && (45) \end{aligned}$$

So,

$$\begin{aligned} \frac{\partial C}{\partial E} &= -\frac{qE}{[E^2 - M^2]^{\frac{3}{2}}}, && (46)\\ &= -C^3 E, && (47) \end{aligned}$$

giving

$$\begin{aligned} \sigma_C^2 &= C^6 E^2 \sigma_E^2, && (48)\\ &= C^4\left(1 + M^2 C^2\right)\sigma_E^2. && (49) \end{aligned}$$

Table 1: Bethe-Bloch parameters used in DeDxBethe.

Parameter	Value
Z/A	0.484 mol/g
I	127.726 eV
C	-3.878
a	0.3123
k	2.878
x_0	0.0966
x_1	2.45
M	139.57 MeV (pion mass)

All other components of the error matrix vanish. If the track parameters are in terms of transverse curvature $C_T = C \sec\lambda$, we get

$$\begin{aligned}
\sigma^2_{C_T} &= \sigma^2_C \sec^2\lambda, && (50)\\
&= C_T^2 C^2 \left(1 + M^2 C^2\right) \sigma^2_E, && (51)\\
&= C_T^4 \cos^2\lambda \left(1 + M^2 C_T^2 \cos^2\lambda\right) \sigma^2_E. && (52)
\end{aligned}$$

Again, all other components of the error matrix vanish.

The implementation of the Bethe-Bloch equation used by DØ and trf can be found in class `DeDxBethe` in d0library package `eloss`. This implementation follows the formulas given in this section except that it uses the approximate form of $T_{\max}$ (Eq. 40). This implementation uses a fixed set of material and incident particle parameters (other than density), which are shown in Table 1. According to the comments in the code, these material parameters are an average of Silicon, Beryllium, Aluminum, and polyvinyl Chloride (I did not check this).

3 The Design and Implementation of `D0Propagator`

The DØ interacting propagator (class `D0Propagator`) differs from ordinary (non-interacting) propagators in that it calculates the effect of material interactions (multiple scattering and energy loss) on track parameters and error matrix. Non-interacting propagators propagage the error matrix reversibly, calculating only the effect of magnetic propagation and coordinate system changes. The interacting propagator adds the irreversible changes from material interactions.

Class `D0Propagator` fulfills the same standard C++ propagator interface as non-interacting propagators. The interacting propagator can in principle be used to propagate to any standard TRF surface in the DØ detector. Attributes of `D0Propagator` include a fully configured dispatching noninteracting propagator (the embedded propagator) that can propagate between any pair of TRF surfaces. `D0Propagator` also maintains a model of the geometry and all of the interacting material in the DØ detector.

Table 2: `D0Propagator` subvolumes.

Class	$r_{\min}$ (cm)	$r_{\max}$ (cm)	$z_{\min}$ (cm)	$z_{\max}$ (cm)	Description
`SMTPropagator`	10^{-15}	20	-84	84	SMT central
`PropSMT_Hdisk`	10^{-15}	29	-127	-84	SMT north
`PropSMT_Hdisk`	10^{-15}	29	84	127	SMT south
`PropCFT`	20	29	-84	84	CFT inner
`PropCFT`	29	53	-127	127	CFT outer
`PropSolenoid`	53	72	-138	138	Solenoid
	72	74	-138	138	CPS
`PropCal`	74	220	-138	138	CC
	10^{-15}	52	-138	-127	FPS north
	10^{-15}	52	127	138	FPS south
`PropCalEC`	10^{-15}	220	-270	-138	EC north
`PropCalEC`	10^{-15}	220	138	270	EC south
	220	1000	-270	270	Muon central
	10^{-15}	1000	-1000	-270	Muon north
	10^{-15}	1000	270	1000	Muon south

The `D0Propagator` geometry and material system divides the volume of the DØ detector into a set of top-level subvolumes, each subvolume having the geometry of a cylindrical shell, or in other words, a rectangle in r-z space. A separate propagator class (a volume specific interacting propagator) is defined for each subvolume. The subvolumes and subvolume propagator classes are shown in Table 2 and Fig. 1. Note that some subvolumes do not have subvolume propagators defined. In these subvolumes, the non-interacting embedded propagator is used, effectively ignoring material in thes subvolumes.

The following is a simplified description of the basic (top-level) algorithm used by `D0Propagator`:

1. Use the embedded non-interacting propagator to propagate to the destination surface. This allows `D0Propagator` to determine the direction of propagation and the (approximate) destination surface and point

2. Determine the current (or newly entered) subvolume.

3. Use the subvolume propagator to propagate toward the destination point, to the destination surface or the subvolume boundary, whichever is closer.

4. If the destination surface has been reached, quit. Otherwise, go back to step 2.

It is the job of each of the subvolume propagators to determine which interacting surfaces or volumes within the subvolume have been crossed, and in which order, to propagate the track to each interacting surface, invoke the interactor for that surface, and finally to propagate to the destination surface. Thus, each subvolume propagator must include among its attributes a model of the material in the subvolume (stored as

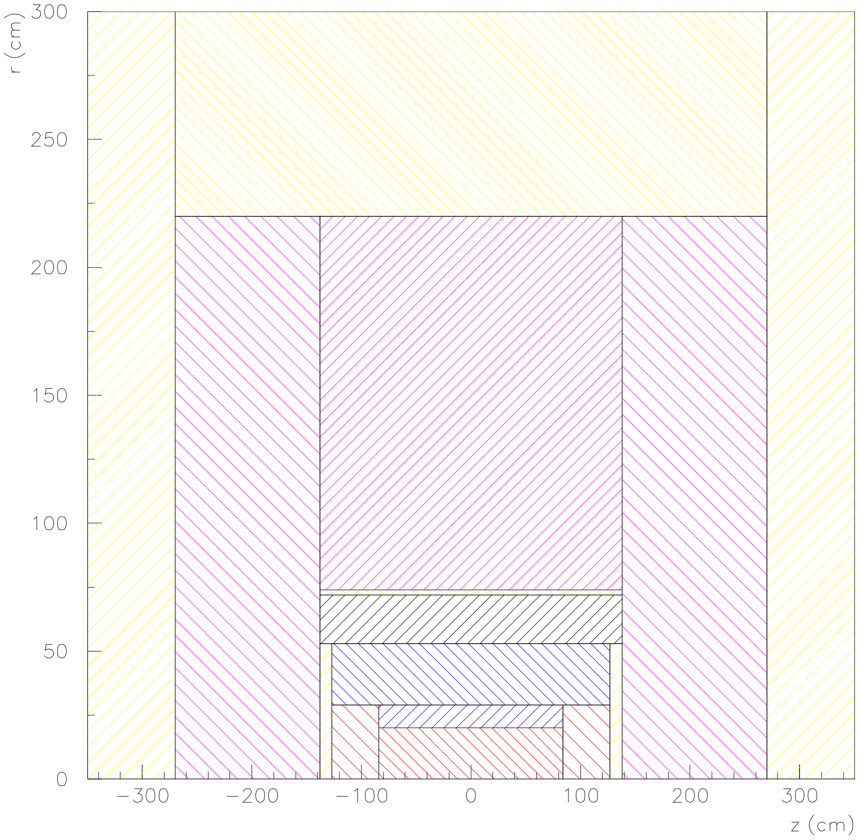

Figure 1: D0Propagator subvolumes.

Table 3: CFT doublets.

Doublet	Radius (cm)	$z_{\max}$ (cm)	Rad. len. (%)	density (g/cm^3)	thickness (cm)
CFTX1	20.079	83.10	0.640	2.265	0.1207
CFTU1	20.248	83.10	0.420	2.265	0.0792
CFTX2	24.989	83.10	0.640	2.265	0.1207
CFTV1	25.158	83.10	0.420	2.265	0.0792
CFTX3	29.889	126.0	0.640	2.265	0.1207
CFTU2	30.058	126.0	0.420	2.265	0.0792
CFTX4	34.799	126.0	0.640	2.265	0.1207
CFTV2	34.969	126.0	0.420	2.265	0.0792
CFTX5	39.709	126.0	0.640	2.265	0.1207
CFTU3	39.879	126.0	0.420	2.265	0.0792
CFTX6	44.619	126.0	0.640	2.265	0.1207
CFTV3	44.789	126.0	0.420	2.265	0.0792
CFTX7	49.519	126.0	0.640	2.265	0.1207
CFTU4	49.689	126.0	0.420	2.265	0.0792
CFTX8	51.519	126.0	0.640	2.265	0.1207
CFTV4	51.689	126.0	0.420	2.265	0.0792

trf interactors). The data for the interactors (including physical dimensions, radiation lengths, density, and thickness) comes from the DØ geometry system.

3.1 PropCFT

Class `PropCFT` is the subvolume propagator for the two CFT subvolumes. Material in the CFT region is modeled as thin cylindrical shells for each of the 16 CFT doublet layers. Multiple scattering and energy loss are both modeled using interactor class `ThinCylMSEloss` (see Appendix A). The parameters of the doublet layers are shown in Table 3. CFT material parameters are stored in rcp file `cft_geometry/rcp/CftMaterialGeometry.rcp`. The material properties for the CFT doublets, as returned by the material geometer, are those of pure graphite (the energy loss interactor uses its own hard-coded material parameters). The geometric parameters of the CFT doublets come from the base geometry.

According to the parameters in Table 3, the total number of radiation lengths in the CFT is 2.15%. The total mass-thickness is 3.6 gm/cm^2.

3.2 SMTPropagator

Class `SMTPropagator` is the subvolume propagator for the central SMT subvolume, which contains the SMT barrels and F disks. The material model for this subvolume includes a) silicon barrels (ladders) b) silicon F-disks, c) the outer SMT support trough, and d) the beampipe. The material model does not include some material, including cables and internal support structures (bulkheads). To compensate for the missing material, the silicon material ge-

Table 4: SMT region material parameters.

Component	Rad. Len. (%)	Density (g/cm^3)	Thickness (cm)	Fudge Factor
Beampipe	0.14	1.85	0.0508	1
Trough	3.00	1.6	0.8	1
Ladder Si Wafer	0.32	2.33	0.03	2.5
F disk Si Wafer	0.32	2.33	0.03	2.5

Table 5: Nominal z positions of SMT ladders and F disks.

SMT element	$z_{\rm min}$ (cm)	$z_{\rm max}$ (cm)
F Disk 1	-53.394	-52.938
F Disk 2	-48.394	-47.938
F Disk 3	-43.394	-42.938
F Disk 4	-38.344	-37.888
Ladder 1	-37.766	-25.766
F Disk 5	-25.532	-25.076
Ladder 2	-24.954	-12.954
F Disk 6	-12.719	-12.263
Ladder 3	-12.141	-0.141
Ladder 4	0.141	12.141
F Disk 7	12.263	12.719
Ladder 5	12.954	24.954
F Disk 8	25.076	25.532
Ladder 6	25.766	37.766
F Disk 9	37.888	38.344
F Disk 10	42.938	43.394
F Disk 11	47.938	48.394
F Disk 12	52.938	53.394

ometry includes fudge factors for the ladder and disk material. Material parameters can be found in `silicon_geometry/rcp/SiMaterialGeometry.rcp` and `d0_geometry/rcp/MaterialGeometry.rcp` in the case of the beampipe. The geometric parameters for the SMT come from the base geometry. Material parameters of the SMT components are shown in Table 4.

3.2.1 SMT Barrels

The SMT barrel detectors are divided in z into six ladder assemblies, each of which contains eight radial silicon layers. Each layer is divided into six or 12 ϕ sections having partial ϕ coverage, with adjacent overlapping layers providing 100% ϕ coverage. The nominal z limits of the six ladder assemblies are shown in Table 5. Nominal radial data of the eight SMT barrels are shown in Table 6. The length of each SMT ladder is 12 cm.

There are a total of 216 ladders of each type (1.92 cm wide and 3.20 cm wide). The

Table 6: SMT barrel layers.

Layer	radius (cm)	ladder width (cm)	N_ϕ	ϕ coverage (%)
1	2.715	1.92	6	64.9
2	3.645	1.92	6	49.2
3	4.550	3.20	6	64.6
4	5.554	3.20	6	53.6
5	6.768	1.92	12	53.8
6	7.758	1.92	12	47.0
7	9.101	3.20	12	66.5
8	10.050	3.20	12	60.3

total area of the SMT ladders is therefore (1.92+3.20) cm$\times$12 cm$\times$216 $= 13,271$ cm^2. The total mass of the SMT ladders (area $\times$ thickness $\times$ density $\times$ fudge factor) is 2.319 kg.

According to the ϕ-coverage parameters in Table 6, a track that is contained in the SMT will intersect, on average, 4.6 ladders. Assuming this number of ladders, at normal incidence (never exactly true, nor even possible) the total number of radiations lengths due to SMT ladders, including fudge factor, is about 3.7%. The total mass-thickness of the SMT ladders is about 0.80 g/cm^2.

3.2.2 SMT F disks

The SMT contains 12 F disk assemblies, six of which are immediately adjacent to the outside end of each of the the six ladder assemblies. Three additional F disk assemblies are located at each end of the central part of the SMT. Each F disk assembly consists of 12 overlapping trapezoidal silicon wedges located on two z planes 0.456 cm apart. The z positions of the F disks are shown in Table 5. The inner and outer radii of F disk assemblies are 2.6 cm and 10.527 cm (wedge height 7.927 cm). The inner and outer widths of the F disk wedges are 1.673 cm and 5.921 cm (average wedge width 3.797 cm).

There are a total of 144 F disk wedges. The total area of the F disk wedges is 7.927 cm $\times$ 3.797cm $\times$ 144 $= 4334$ cm^2. The total mass of the SMT F disk wedges is (area $\times$ thickness $\times$ density $\times$ fudge factor) 0.757 kg.

3.2.3 SMT Support Trough and Beampipe

The other major structures that are included in the material model of the SMT are the SMT support trough and beampipe. The beampipe is a beryllium cylinder with a radius of 1.905 cm (0.75") and extending in z to $\pm$118.9 cm. The SMT support trough is a cylinder that surrounds the SMT. The SMT trough is made of carbon. It has a radius of 15.0 cm and extends in z to $\pm$50 cm.

Table 7 gives some total or average material parameters for the four components of the SMT material model.

Table 7: Average and total material parameters of SMT and CFT.

Component	Rad. Len. (%)	Mass-thickness (g/cm^2)	Mass (kg)
Beampipe	0.14	0.094	0.267
Trough	3.00	1.28	12.063
SMT Ladders	3.68	0.80	2.319
SMT F disks			0.757
SMT (Ladders + F disks)	3.68	0.80	3.076
SMT + Trough + Beampipe	6.82	2.17	15.406
CFT	2.15	3.62	

A TRF interactor classes

TRF interactor classes are listed in Table 8. Here are brief descriptions of the interactor classes.

A.1 Interactor

Class `Interactor` is the interactor base class. This class provides the following two virtual methods as its interface.

```
virtual void interact(ETrack& tre) const =0;
virtual void interact_dir(ETrack& tre, const int direction) const;
```

`Interactor` does not contain any data. The directional interaction method has a default implementation, which is to call the nondirectional method (i.e. the direction is ignored). Concrete interactors which need direction information must override the directional method. The directional method is the one that is called in `D0Propagator`. Direction information is only needed by energy loss interactors, or in general by interactors that modify the mean values of the track parameters. Interactors that do not modify track parameter values, including multiple scattering interactors, do not need direction information. Note that regardless of the direction of propagation, the error is always increased by an interactor.

A.2 MultiInteractor

Class `MultiInteractor` is a collection of interactors. Its function consists of calling each interactor in sequence. `MultiInteractor` only implements the nondirectional interaction method (this is arguably a bug), thus `MultiInteractor` should only be used with nondirectional interactors. This class is no longer used in the interacting propagator, having been replaced by `ThinCylMSEloss`.

A.3 Thin multiple scattering interactors

Thin multiple scattering interactors exist for all three physical trf surfaces (cylinder, z-plane, and xy-plane). These interactors implement the nondirectional interaction

Table 8: TRF interactor classes.

Class	Package	Description
`trf::Interactor`	`trfbase`	Interactor base class.
`trf::MultiInteractor`	`trfbase`	Compound interactor.
`trf::ThinCylMS`	`trfcyl`	Thin cylinder multiple scattering
`trf::ThinXYPlaneMS`	`trfxyp`	Thin xy-plane multiple scattering
`trf::ThinZPlaneMS`	`trfzp`	Thin z-plane multiple scattering
`trf::ThickCylMS`	`trfcyl`	Thick cylinder multiple scattering
`trf::ThickZPlaneMS`	`trfzp`	Thick z-plane multiple scattering
`trf::CylEloss`	`trfcyl`	Thin cylinder energy loss
`trf::ThinCylMSEloss`	`trfcyl`	Thin cylinder MS + energy loss

method. Data consists of the number of radiation lengths. Multiple scattering interactors only modify the track errors associated with track direction parameters.

A.4 Thick multiple scattering interactors

Thick multiple scattering interactors exist for cylinders and z-planes (the xy-plane thick multiple scsttering interactor is omitted). These interactors implement the nondirectional interaction method. Data consists of the number of radiation lengths plus the physical path length in centimeters. Multiple scattering interactors only modify the track errors.

A.5 Energy loss interactors

Energy loss interactors exist only for thin cylinders. These interactors override the directional interaction method. Data consists of thickness and density of the material.

References

[1] H. Greenlee, DØ Note 4180.

[2] K. Hagiware *et al.* (Particle Data Group), Phys. Rev. D **66**, 010001 (2002).

[3] H. Bichsel, Chapter 87 in *Atomic, Molecular and Optical Physics Handbook*, G.W.F. Drake, ed., Am. Inst. Phys. Press, Woodbury, NY, 1996.